ADVANCED FUNCTIONAL MATERIALS

Supporting Information

for *Adv. Funct. Mater.,* DOI: 10.1002/adfm.202203889

Highly-Packed Proximity-Coupled DC-Josephson Junction Arrays by a Direct-Write Approach

Fabrizio Porrati, Felix Jungwirth, Sven Barth, Gian Carlo Gazzadi, Stefano Frabboni, Oleksandr V. Dobrovolskiy, and Michael Huth*

Highly-packed proximity-coupled DC-Josephson junction arrays by a direct-write approach

Fabrizio Porrati[1], Felix Jungwirth[1], Sven Barth[1], Gian Carlo Gazzadi[2], Stefano Frabboni[2,3], Oleksandr V. Dobrovolskiy[4], and Michael Huth[1]

1. Physikalisches Institut, Goethe-Universität, Max-von-Laue-Str. 1, D-60438 Frankfurt am Main, Germany

2. S3 Center, Nanoscience Institute-CNR, Via Campi 213/a, I-41125 Modena, Italy

3. FIM Department, University of Modena and Reggio Emilia, Via G. Campi 213/a, I-41125 Modena, Italy

4. Faculty of Physics, University of Vienna, Boltzmanngasse 5, A-1090 Vienna, Austria

Keywords: focused ion beam induced deposition, direct-write fabrication, nanolithography, NbC, superconductor-to-metal transition, magnetic frustration, Josephson junction arrays

Supporting Information

Microdiffraction on single grains

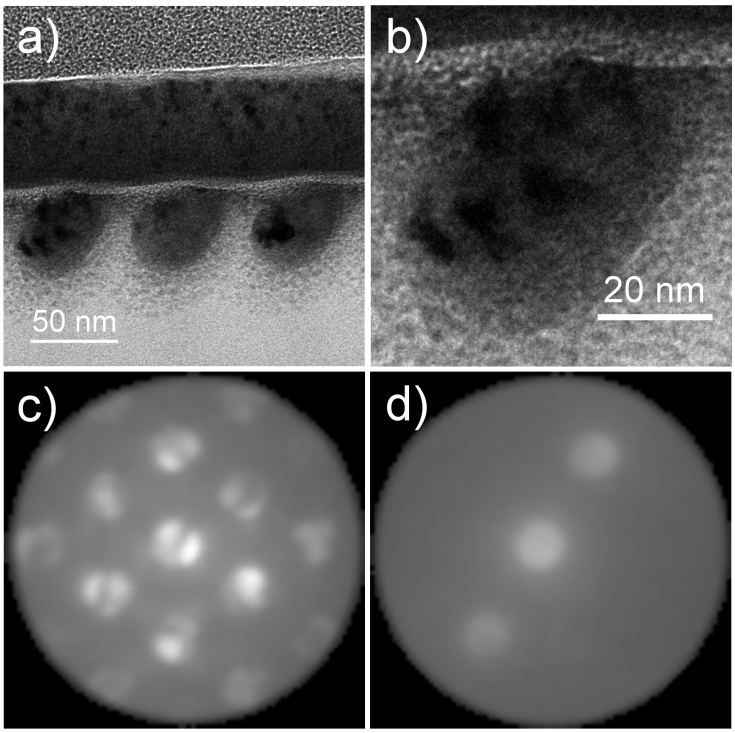

Figure S1: a) Bright-field image of the sample-lamella $t2$. Three dots are visible, covered by a Co_3Fe/PtC protective double-layer grown by FEBID/FIBID. b) Zoom-in on one dot. Grains of 10-20 nm size are present inside. Microdiffraction carried out on Si [110] for calibration (c) and on single dot-grain (d). The diffraction image is compatible with NbC (111). This is found by comparing the ratio of the atomic planes of Si and NbC, respectively d_{Si}=5.43 $\mathring{A}$ and d_{NbC}=4.47 $\mathring{A}$[1], i.e. R=1.21, with the ratio of the center-to-center distances of neighboring reflexion points of the diffraction images (d) and (c), respectively. Flucam was used to avoid contaminations during data acquisition.

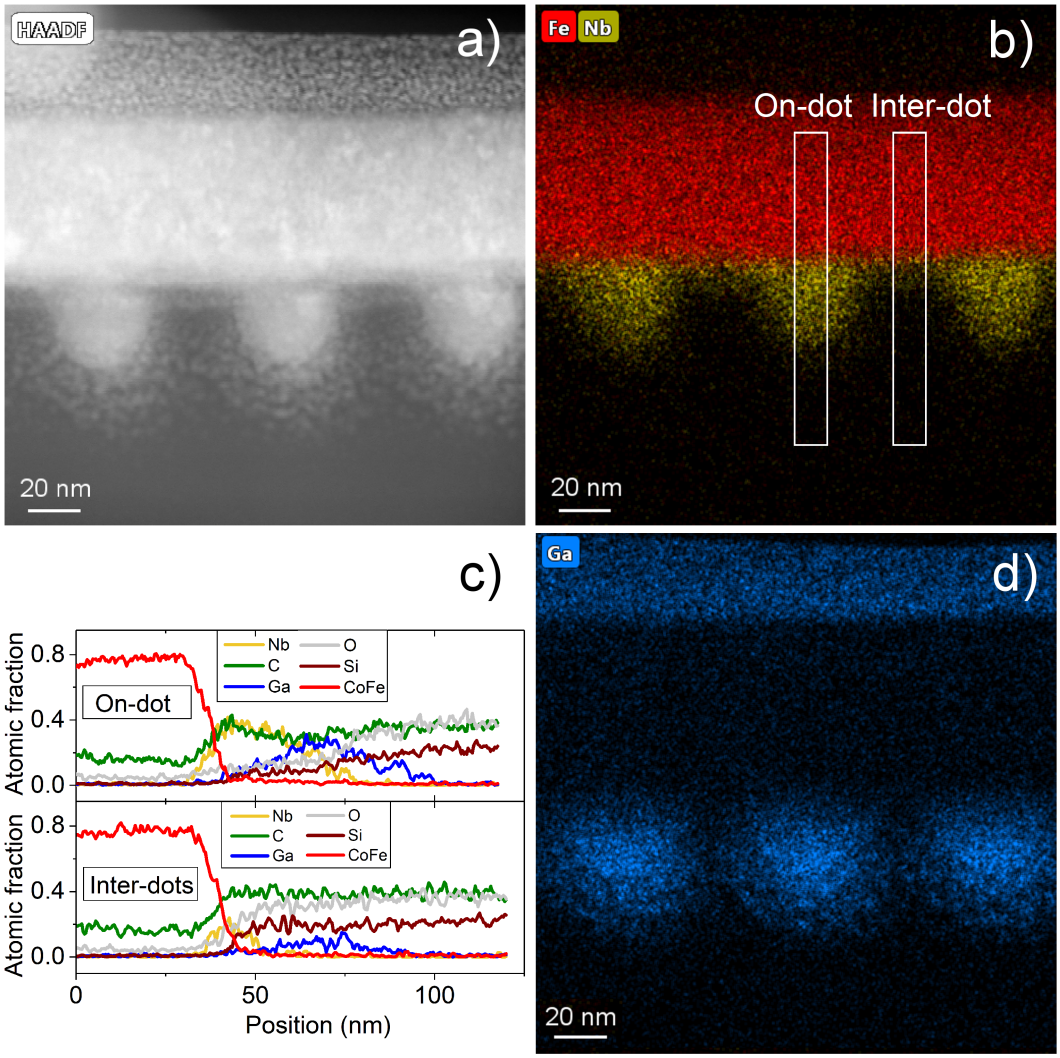

Figure S2: (a) STEM-HAADF image of a series of dots with thickness 30 nm and with inter-dot distance equal to 70 nm. (b), (d) 2D STEM-EDS compositional analysis of the dot region. The images show the spatial distribution of Nb and Ga. (c) Line-scans of the inter-dot and on-dot regions.

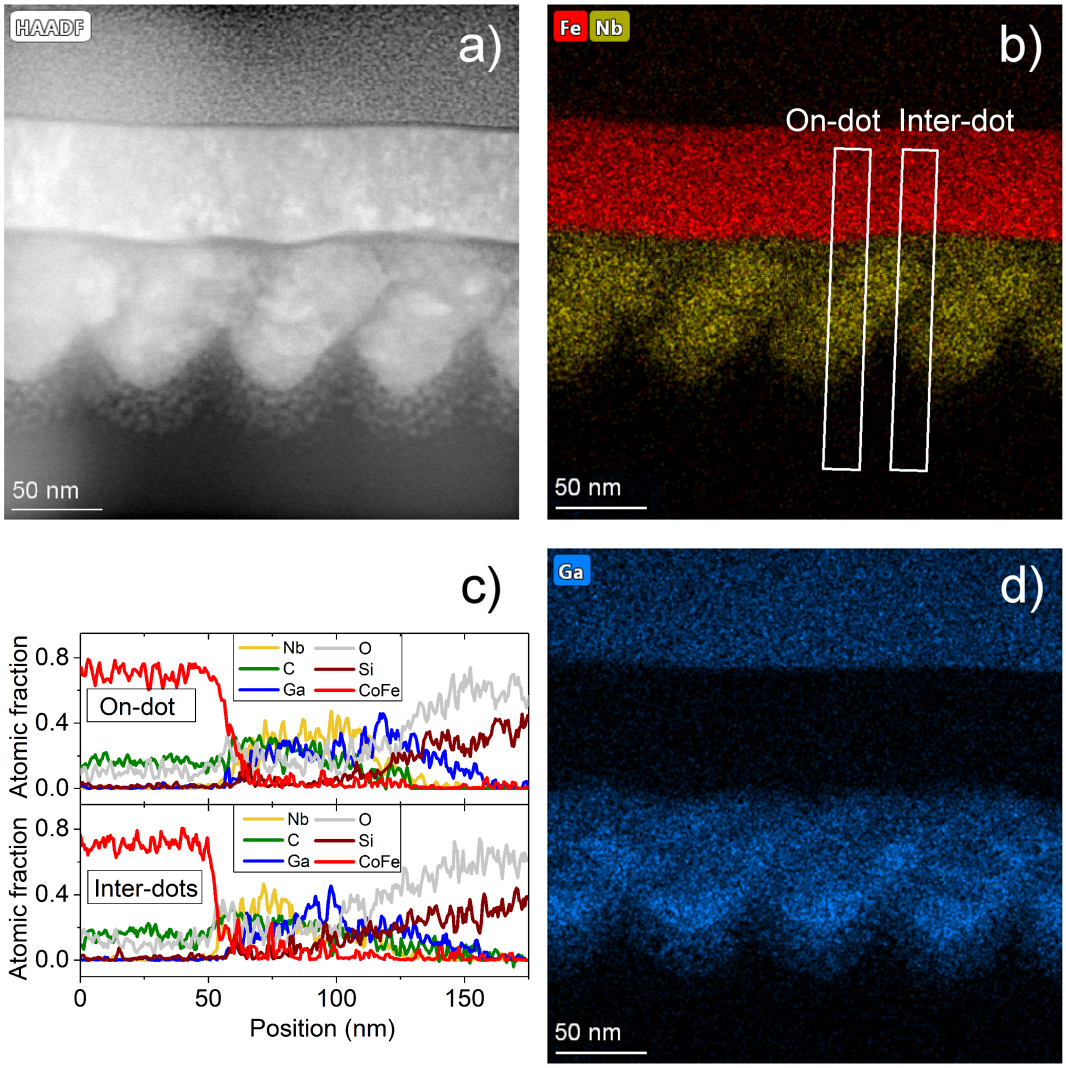

Figure S3: (a) STEM-HAADF image of a series of dots with thickness 90 nm and with inter-dot distance equal to 70 nm. (b), (d) 2D STEM-EDS compositional analysis of the dot region. The images show the spatial distribution of Nb and Ga, respectively. (c) Line-scans of the inter-dot and on-dot regions.

Critical resistance at the metal-insulator transition. In the past decades, the insulator-(metal)-superconductor quantum phase transition was investigated in homogeneous films, granular films, Josephson-junction arrays and nanowires. In several systems, like Pb, Sn, Al, In, and Ga thin films[2,3] the transition occurs if the sheet resistance is close to the quantum resistance, $R_\square \approx R_Q = h/(2e)^2$, as predicted by the dirty boson model[4]. However, other systems, for example α-MoGe thin films, do not show this dependence[5]. Therefore, $R_\square$ is not considered as the unique parameter to control the transition. For example, in nanowires, the parameter to tune the SIT is the normal resistance[6,7]. In SIS Josephson junction arrays the driving parameter is the ratio E_J/E_c between Josephson coupling energy and charging energy[8]. In the present investigation, we use the normal resistance R_N to describe the transition, see Fig. S5. In particular, the samples can be divided in two groups: those with normal state resistance $R_N < R_Q$, see samples s10 and s12, which are expected to become superconducting at low temperatures, and those with $R_N > R_Q$, i.e. samples s3, s4 and s7.

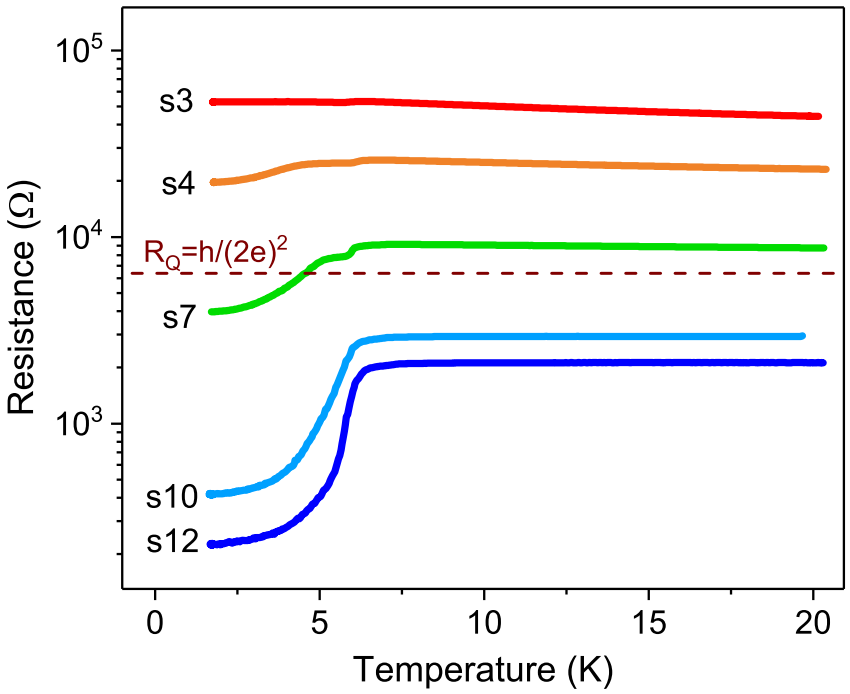

Figure S4: Low temperature dependence of the resistance for the series of samples investigated in the present work.

Criterion used to determine the temperatures T_1 and T_2

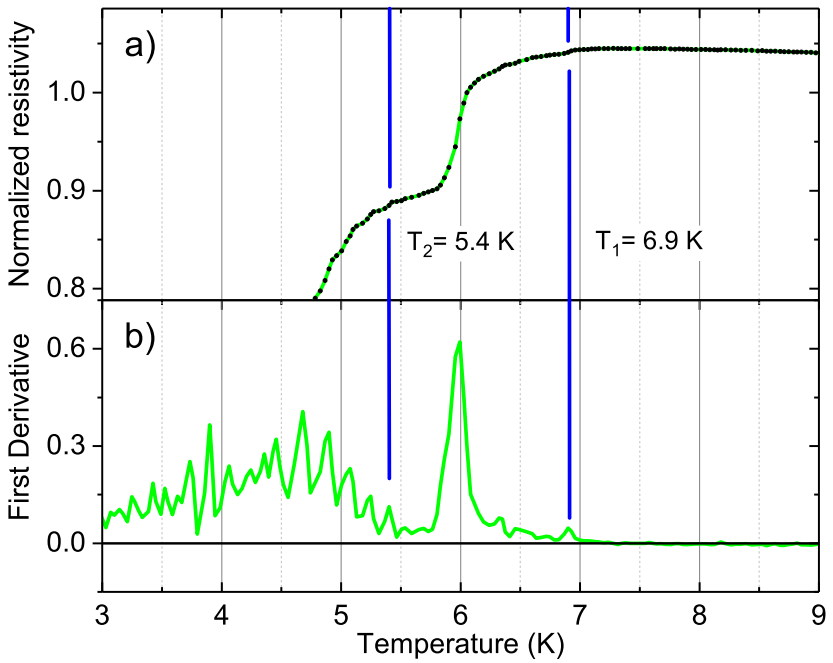

Figure S5: The criterion is based on the analysis of the RT curve (a) and of its first derivative (b) at low temperature. This is shown exemplary for s7. Down to 7 K RT slightly increase monotonically and the derivative is constant. At 6.9 K RT shows a first step down, visible by a peak in the first derivative, which mark the temperature T_1 for which local phase coherence starts to set in the NbC dots. The process ends at about 5.7 K, where all the NbC dots are superconducting. At lower temperatures global phase coherence develops, which takes place with a series of steps, represented by peaks in the derivative. The temperature of the first peak in this regime is marked as T_2, in the example at 5.4 K.

Comparison between two- and four-probe measurements

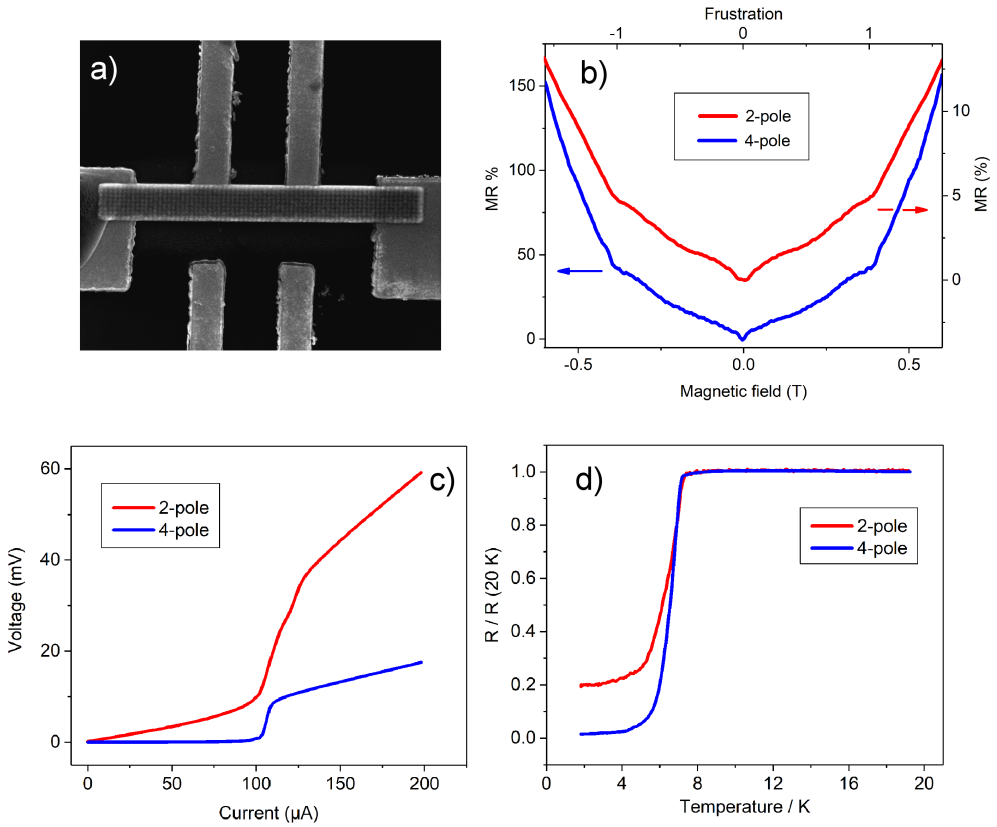

Figure S6: (a) NbC array wired with Au-electrodes for two- and four-probe transport measurements. The thickness of the sample, about 40 nm, is such that only slight oscillations are visible in the MR curve. (b) MR measured at 1.5 K. The dips of the oscillations locate in the same position in the two measurements. This justifies the choice to study the oscillations of NbC-arrays with the two-probe configuration. (c) Comparison of the I-V characteristics taken at 1.5 K. (d) Temperature dependence of the normalized resistance R(20 K)/ R resistance. A residual resistance is present in the two-probe measurement, which disappears in the four-probe measurement.

Comparison between protected and unprotected samples

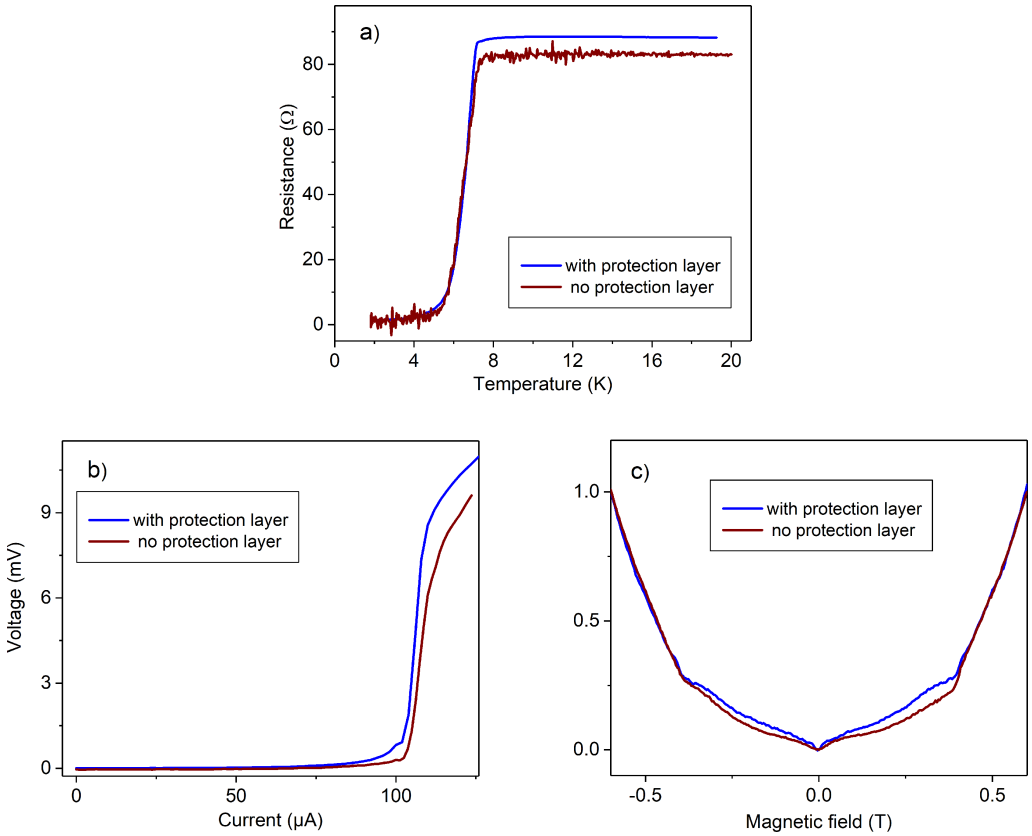

Figure S7: In Figure (a) is depicted the low temperature RT curve of the samples. At 20 K the 4-pole resistance are 88 Ω and 82 Ω for protected and non protected samples, respectively. Moreover, the non protected sample appears noisy, which might be due to oxidation effects. However, the superconducting properties of the samples are similar: Tc≈6.5 K, Ic≈103 μA, protected (104 μA, non protected), see Figure (b). Furthermore, the slight oscillation visible in the RB curve, Figure (c), are located at the same position. In particular, a dip is observed at 0.38 T, which correspond to the value of frustration equal to one. The comparison shows that the superconducting properties of the arrays are not altered by the presence of the protective layer.

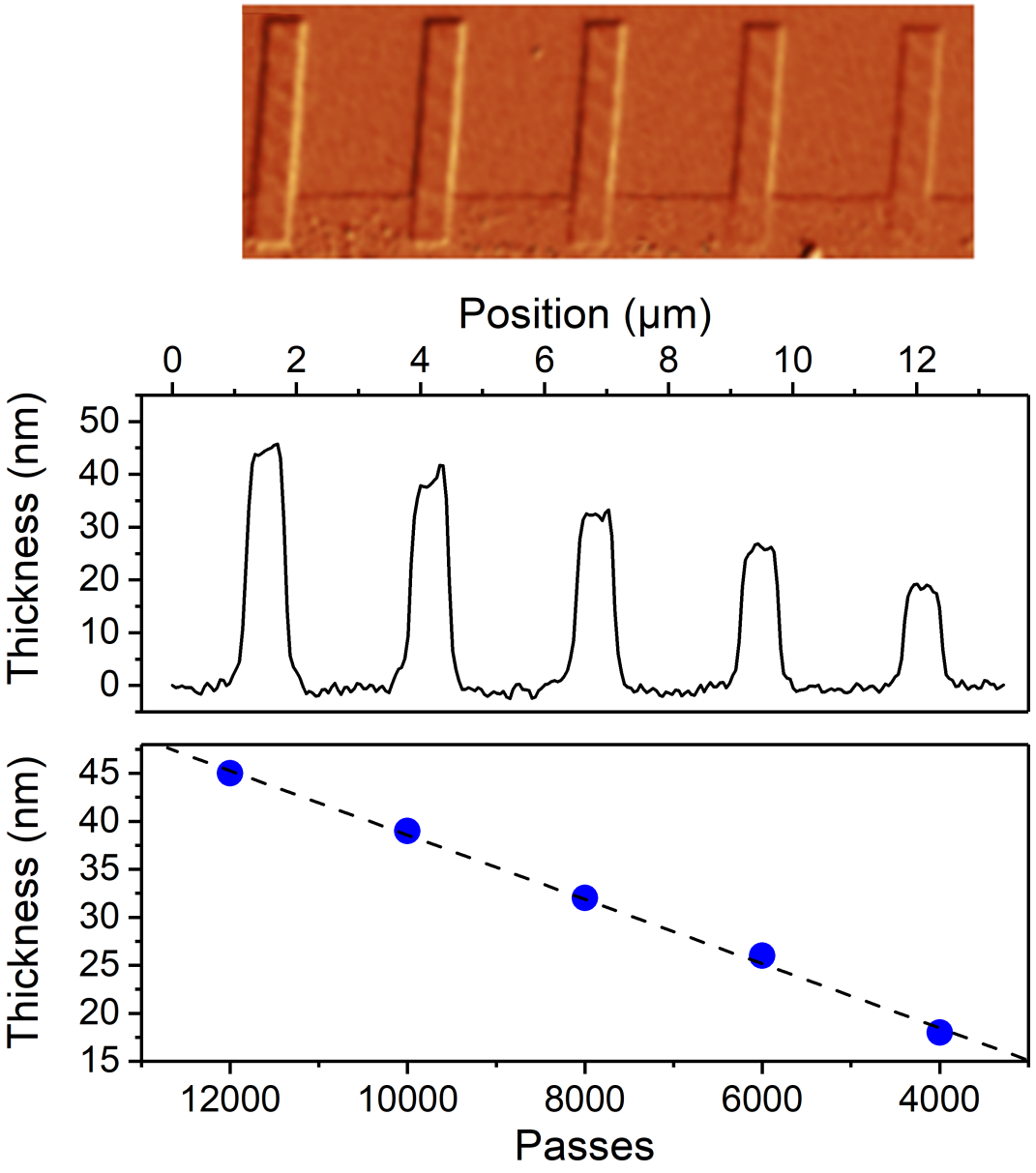

Figure S8: Calibration of the thickness of the dc-Josephson junction arrays. A series of samples was grown with ion beam parameters as reported in the paragraph "Fabrication" in main text, with variable number of passes attached to a gold electrode. The thickness was measured by atomic force microscopy (AFM) in non-contact mode. The fine-structure of the sample (dots) is not visible due to the large scan area.

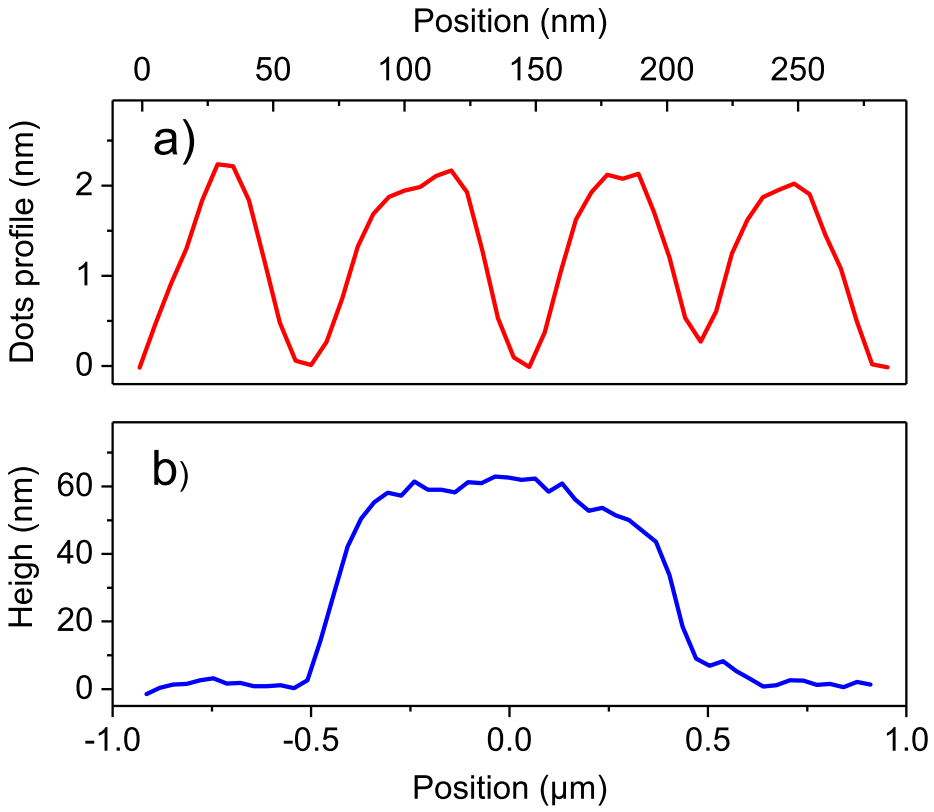

Figure S9: (a) AFM measurement of the fine-structure of the dots for a sample with thickness of 55 nm (b).

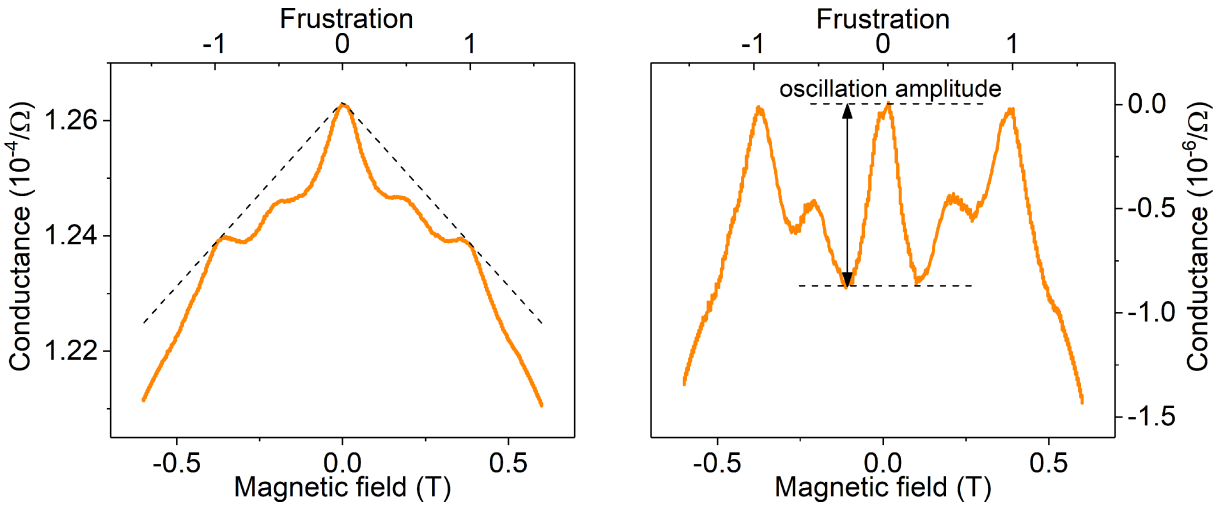

Figure S10: Background subtraction to determine the conductance oscillation amplitude.

References

[1] R. W. G. Wyckoff, *Crystal Structures - Volume 1*, Interscience Publishers, **1963**.

[2] H. M. Jaeger, D. B. Haviland, B. G. Orr, A. M. Goldman, *Phys. Rev. B* **1989**, *40* 182.

[3] D. B. Haviland, Y. Liu, A. M. Goldman, *Phys. Rev. Lett.* **1989**, *62* 2180.

[4] M. P. A. Fisher, *Phys. Rev. Lett.* **1990**, *65* 923.

[5] A. Yazdani, A. Kapitulnik, *Phys. Rev. Lett.* **1995**, *74* 3037.

[6] A. Bezryadin, C. N. Lau, M. Tinkham, *Nature* **2000**, *404*, 6781 971.

[7] A. T. Bollinger, A. Rogachev, M. Remeika, A. Bezryadin, *Phys. Rev. B* **2004**, *69* 180503.

[8] H. S. J. van der Zant, W. J. Elion, L. J. Geerligs, J. E. Mooij, *Phys. Rev. B* **1996**, *54* 10081.